Biochimica et Biophysica Acta 1844 (2014) 576–584

Contents lists available at ScienceDirect

Biochimica et Biophysica Acta

journal homepage: www.elsevier.com/locate/bbapap

FAD binding properties of a cytosolic version of *Escherichia coli* NADH dehydrogenase-2

Josefina M. Villegas [a], Lorena Valle [b], Faustino E. Morán Vieyra [b], María R. Rintoul [a], Claudio D. Borsarelli [b,*], Viviana A. Rapisarda [a,*]

[a] Instituto de Química Biológica "Dr Bernabé Bloj", Facultad de Bioquímica, Química y Farmacia (UNT) and Instituto Superior de Investigaciones Biológicas, INSIBIO, CCT-Tucumán (CONICET-UNT), Chacabuco 461, T4000ILI Tucumán, Argentina

[b] Laboratorio de Cinética y Fotoquímica, Centro de Investigaciones y Transferencia de Santiago del Estero (CITSE-CONICET), Universidad Nacional de Santiago del Estero (UNSE), RN9 Km 1125, Villa el Zanjón, 4206 Santiago del Estero, Argentina

ARTICLE INFO

Article history:
Received 21 October 2013
Received in revised form 27 December 2013
Accepted 31 December 2013
Available online 10 January 2014

Keywords:
NADH dehydrogenase
FAD
Flavoprotein
Fluorescence
Flavin binding

ABSTRACT

Respiratory NADH dehydrogenase-2 (NDH-2) of *Escherichia coli* is a peripheral membrane-bound flavoprotein. By eliminating its C-terminal region, a water soluble truncated version was obtained in our laboratory. Overall conformation of the mutant version resembles the wild-type protein. Considering these data and the fact that the mutant was obtained as an apo-protein, the truncated version is an ideal model to study the interaction between the enzyme and its cofactor. Here, the FAD binding properties of this version were characterized using far-UV circular dichroism (CD), differential scanning calorimetry (DSC), limited proteolysis, and steady-state and dynamic fluorescence spectroscopy. CD spectra, thermal unfolding and DSC profiles did not reveal any major difference in secondary structure between apo- and holo-protein. In addition, digestion site accessibility and tertiary conformation were similar for both proteins, as seen by comparable chymotryptic cleavage patterns. FAD binding to the apo-protein produced a parallel increment of both FAD fluorescence quantum yield and steady-state emission anisotropy. On the other hand, addition of FAD quenched the intrinsic fluorescence emission of the truncated protein, indicating that the flavin cofactor should be closely located to the protein Trp residues. Analysis of the steady-state and dynamic fluorescence data confirms the formation of the holo-protein with a 1:1 binding stoichiometry and an association constant $K_A = 7.0(\pm 0.8) \times 10^4\ M^{-1}$. Taken together, the FAD–protein interaction is energetically favorable and the addition of FAD is not necessary to induce the enzyme folded state. For the first time, a detailed characterization of the flavin:protein interaction was performed among alternative NADH dehydrogenases.

1. Introduction

Many proteins require the binding of a non-covalently bound ligand to be functional. The ligand, or cofactor, can vary from a simple metal ion to an organic molecule. Sometimes, the presence of a cofactor is necessary to acquire the correct folding of a protein [1,2]. On the other hand, it is also possible that the cofactor binds to the protein when it is already folded, without major structural changes [3].

Flavoprotein family embraces an enormous amount of enzymes catalyzing a variety of reactions utilizing flavin mononucleotide (FMN) or flavin adenine dinucleotide (FAD) as noncovalently or covalently bound cofactors [4–6]. They have a central role in aerobic metabolism through their ability to catalyze both one- and two-electron transfer reactions. Type II NADH dehydrogenase (NDH-2), a membrane-bound flavoprotein, belongs to the pyridine nucleotide disulfide reductase (PNDR) protein family and catalyzes the electron transfer from NADH to quinones without energy transduction [7,8]. NDH-2s are found in a broad range of organisms including plants, fungi, protozoa, and bacteria, but crucially, not in mammalian mitochondria [9–12]. Due to this fact, they were studied as potential therapeutic targets against human pathogens such as *Plasmodium falciparum* [13–15] and *Mycobacterium tuberculosis* [16,17]. On the other hand, *Saccharomyces cerevisiae* homologue Ndi1 has been proposed as substitute in gene therapy since it complements deficiencies in respiratory complex I of human cell cultures [18–21].

Respiratory NDH-2 of *Escherichia coli* has been biochemically characterized [22,23]. It consists of a single polypeptidic chain of 433 residues (47.2 kDa), containing a non-covalently bound FAD as redox cofactor [23]. Even though the crystal structure of *S. cerevisiae* Ndi1 has been recently reported [24,25], *E. coli* NDH-2 structural features were restricted to bioinformatics information [26,27] and experimental data obtained with low-resolution techniques [28,29].

In earlier works, we demonstrated that NDH-2 is a peripheral membrane protein with its C-terminal region as responsible for membrane

* Corresponding authors.
E-mail addresses: cdborsarelli@gmail.com (C.D. Borsarelli), vrapisarda@fbqf.unt.edu.ar (V.A. Rapisarda).

1570-9639/$ – see front matter © 2014 Elsevier B.V. All rights reserved.
http://dx.doi.org/10.1016/j.bbapap.2013.12.021

binding [28]. A cytosolic variant of NDH-2 (named as Trun-3), which was truncated in the last 43 amino acids, was purified and characterized [28]. Trun-3 lacked flavin cofactor, even though it contains the conserved FAD binding domain and motifs [27,30]. Thus, apo-Trun-3 was inactive but after cofactor addition immediately restored its enzymatic activity, with the same substrate affinity as the wild-type enzyme [28]. In addition, the elimination of the C-terminal region did not affect NDH-2 globularity, since no significant differences in the overall topology of NDH-2 and reconstituted holo-Trun-3 were observed by far-UV circular dichroism, Fourier transform infrared spectroscopy and limited proteolysis analysis [29].

Trun-3 was proposed as a suitable testing model to study unknown structural/functional aspects of NDH-2 [28,29]. The usage of this soluble version avoided the several difficulties related to handle the native membrane protein [31]. Till date, no information about achievement of apo-Type II NADH dehydrogenase is available, indicating the complexity of this approach. Several attempts to deflavonize *E. coli* NDH-2 failed, as reconstitution with the FAD cofactor resulted in an inactive protein [23; Rapisarda et al., unpublished data]. Thus, Trun-3 version offers a good opportunity to characterize the cofactor–protein interaction, since it is possible to prepare large amounts of a stable and reconstitutable apo-protein with nearly the same structural properties to those of native enzyme.

In the present study, structural properties of apo- and holo-forms of Trun-3 were investigated by far-UV circular dichroism and limited proteolysis analysis. The FAD binding equilibrium constant of type-2 NADH dehydrogenase was determined by steady-state and time-resolved fluorescence measurements. This is the first time that the flavin–apoprotein interaction was characterized for any alternative NADH dehydrogenase.

2. Materials and methods

2.1. Chemicals and media

All chemicals and growth medium were purchased from Sigma-Aldrich (St. Louis, MO, USA).

2.2. Protein expression and purification

Expression of His-tagged Trun-3 protein was induced with 0.1 mM IPTG in early log phase cultures of BLTrun-3 strain [28]. Briefly, the protein was purified by affinity chromatography using a Ni-NTA column following the protocol adapted by Villegas et al. [28]. Purified protein that lacked FAD cofactor was named as apo-Trun-3 and the reconstituted holo-form, after the addition of FAD excess, was named as holo-Trun-3. All assays were performed in 50 mM potassium phosphate buffer, pH 7.5, containing 0.5 M NaCl. Protein concentration was determined by the method of Lowry et al. [32].

2.3. Limited proteolysis

Samples (0.5 mg ml^{-1}) were incubated with bovine pancreas chymotrypsin at 30 °C (protease/protein ratio 1:30). Reaction was stopped after 5, 15 and 60 min by adding SDS-PAGE loading buffer and boiling at 100 °C for 5 min. Proteolysis reaction products were analyzed by 10% SDS-PAGE [33], and stained with Coomassie Blue. When indicated, 4-fold molar excess of FAD was added to the protein sample.

2.4. Circular dichroism

Far-UV circular dichroism (CD) spectra were performed with a Jasco 810 spectropolarimeter under constant N_2 flush, equipped with a Haake temperature control unit. Scans were carried out in a 2 mm path length quartz cuvette at a speed of 100 nm min^{-1}, a band width of 1 nm, a data pitch of 0.2 nm s^{-1} and a response time of 1 s. When indicated, 4-fold molar excess of FAD was added to the protein sample. Buffer scans were subtracted from the protein spectra. The results were expressed as mean residual ellipticity [θ], given in deg cm^2 $dmol^{-1}$, and calculated by Eq. (1),

$$[\theta] = \frac{\theta \times 100 \times M}{C \times l \times n} \quad (1)$$

where θ is the observed ellipticity, M is the molecular mass, C is the sample concentration in mg ml^{-1}, l the optic length in cm, and n is the number of residues in the protein [34].

2.5. Differential scanning calorimetry

Calorimetric experiments were obtained using a MicroCal VPDSC calorimeter from MicroCal Llc. (Northampton, MA, USA). The protein concentration was 0.5 mg ml^{-1}. All the solutions were degassed by vacuum. The reference cell was filled with buffer and a pressure of 26 psi was applied to both cells. A scan rate of 60 °C/h was used in all experiments. Buffer–buffer scan was subtracted to the crude sample scan and subsequently normalized for total protein concentration. The experimental data were deconvoluted using Origin software provided by the manufacturer. A non-two-state transition analysis was applied, previous baseline subtraction, to obtain the thermal transition midpoint (T_m).

2.6. Steady-state UV–vis absorption and fluorescence

Absorption UV–vis spectra were registered with a Hewlett Packard 8453 UV–visible spectrophotometer (Palo Alto, CA, USA). Fluorescence excitation and emission spectra were recorded with a Hitachi F-2500 spectrofluorimeter (Kyoto, Japan) equipped with an R-928 photomultiplier, in a 100 μl fluorescence quartz cell of 3 mm of optical path cells (Hellma, Germany), using excitation and emission slits of 5 nm bandwidth. Fluorescence titration of FAD binding to the apoprotein was determined by excitation of the flavin at 450 nm, and the respective FAD quantum yield (Φ_F) was calculated using, as reference, the fluorescence of the cofactor in buffer solution ($\Phi_F = 0.033$) [35], by comparing the integrated fluorescence intensity of the sample and reference solutions matched in absorbance at the excitation wavelength. Correction by the difference of the media refractive index was performed and the absorbance of both sample and reference solutions at 450 nm was kept ≤0.05 to avoid inner filter effects [35].

The steady-state quenching of Trun-3 intrinsic fluorescence by addition of FAD was studied by excitation at 295 ± 5 nm, and the emission spectra were recorded between 300 and 450 nm. Since FAD absorbs light both at the excitation and emission spectral regions of Trun-3, the observed emission spectra, $F(\lambda)_{obs}$, were corrected by the primary and secondary inner filter effects using Eq. (9) [36],

$$F(\lambda_{em})_{corr} = F(\lambda_{em})_{obs} \text{anti log}\left(\frac{A(\lambda_{ex}) + A(\lambda_{em})}{2}\right) \quad (2)$$

where $A(\lambda_{ex})$ and $A(\lambda_{em})$ are the absorbance of the solution upon addition of different FAD concentrations at the excitation and emission ranges, respectively.

Steady-state fluorescence anisotropy r was determined using the classical L-format and calculated with Eq. (3), where I_{VV} and I_{VH} are the fluorescence intensities with different orientations of the excitation and emission polarizers, indicating the position by the subscripts V (vertical) and H (horizontal), respectively. The G factor represents the sensitivity ratio of the detection system for vertically and horizontally polarized light calculated as I_{HV}/I_{HH}.

$$r = \frac{I_{VV} - GI_{VH}}{I_{VV} + 2GI_{VH}} \quad (3)$$

Changes of the steady-state anisotropy of FAD, r^{FAD}, as a function of the Trun-3 concentration were calculated using the red-edge fluorescence intensity collected between 560 and 620 nm with excitation at 450 nm, in order to avoid light scattering effects that are compounded at the blue edge of the spectrum at increasing concentrations of the apo-protein. In turn, the anisotropy of 10 μM apo-protein in buffer solution, r^{Apo}, was calculated by excitation at 295 nm and collecting the emission between 300 and 450 nm. In all cases, the average value of anisotropy in the studied range is reported.

2.7. Time-resolved fluorescence measurements

Fluorescence emission decays of the apo-protein were obtained with a Tempro-01 apparatus of Horiba (Glasgow, UK), using as excitation source 1 MHz pulsed LEDs (Nanoled® from Horiba) emitting at 277 ± 11 nm. The emission wavelength was selected at 340 ± 16 nm, through an f/4 monochromator. The fluorescence intensity decay was fitted with the Fluorescence Decay Analysis Software DAS6® from Horiba by deconvolution of the pulse function using the multi-exponential model function (Eq. (4)),

$$I(t) = \sum_{i=1}^{n} \alpha_i \exp(-t/\tau_i) \quad (4)$$

where n is the number of single exponential decays, τ_i and α_i are the decay time and the fluorescence intensity amplitude at $t = 0$ of each decay, respectively. The average lifetime (τ_{av}) was calculated with Eq. (5), where f_i is the fractional contribution of each decay time to the steady-state intensity [36].

$$\tau_{av} = \sum_{i=1}^{n} f_i \tau_i = \frac{\sum_{i=1}^{n} \alpha_i \tau_i^2}{\sum_{i=1}^{n} \alpha_i \tau_i} \quad (5)$$

All spectroscopic measurements were performed under air-saturated conditions and controlled temperature at 30 ± 0.1 °C using an external thermostat (Haake F3, Germany).

3. Results and discussion

3.1. Apo- and holo-Trun-3 structural features

Based on spectroscopic experiments, it was previously shown that holo-Trun-3 retained a compact fold with a high degree of native-like secondary structure. Furthermore, limited proteolysis experiments demonstrated a comparable tertiary structure, indicating that the overall conformation of Trun-3 resembles the wild-type protein [29]. Also, the similar K_m values obtained showed that the substrate binding site(s) of both enzymes remain unchanged [28]. These data, complemented with the fact that Trun-3 was obtained as an apo-protein (apo-Trun-3), allowed us to propose this variant as an ideal model for studying the binding between the protein and the cofactor, overcoming the difficulties related to the native NDH-2 handle. Here, in order to elucidate if structural rearrangements could be induced exclusively by the cofactor addition, comparative studies between apo- and holo-Trun-3 were performed. Far-UV circular dichroism spectroscopy (λ < 250 nm) was used to estimate possible modifications in the secondary structure of Trun-3 by addition of FAD. At 30 °C, the CD-spectra of both apo- and holo-protein were very similar, showing a characteristic α/β pattern [37], as indicated by the broad negative band with maxima centered at 208 and 222 nm, together with a positive band slightly red-shifted at 201 nm (Fig. 1A). As observed in the difference spectrum between the holo- and apo-protein (inset of Fig. 1A), only a very small signal increment was observed at 204 nm, probably by a slight increased contribution of type I β-turn in the holo-protein [37]. These results indicate that the conformation adopted by the apo-protein is not strongly influenced by the binding of the flavin cofactor, and reinforce the assertion that the structure of both apo and holo-forms of the mutant enzyme is overall very similar to that of wild-type protein. In addition, both apo- and holo-proteins showed the same thermal stability of the secondary structure, as monitored by the changes of the normalized ellipticity at 222 nm (Fig. 1B). No significant changes were observed up to 41 °C. An apparent midpoint transition temperature (T_m) of 48.8 ± 1 °C was obtained by fitting with a Boltzmann model [38]. To further characterize the thermal transitions of apo and holo-Trun-3, high-sensitivity differential scanning calorimetry (DSC) measurements were carried out. Both calorimetric scans consisted of three entities melting at different temperatures. The lower transition peak for the apo-protein had a T_m of 41.5 ± 0.5 °C (Fig. 1C), while the holo- form showed a T_m of 43.5 ± 0.7 °C (Fig. 1D). The other peaks were located at 50 and 53 °C for both proteins, being the last one the higher transition peak. Considering the CD and DSC results, it can be concluded that both proteins show similar thermal unfolding profiles and therefore the binding of FAD does not significantly modify the stability of Trun-3 structure. However, slight structural modifications upon flavin addition cannot be discarded upon formation of the holo-protein. The effect of FAD binding on possible changes of the protein tertiary structure was investigated by chymotryptic limited digestion. As shown in Fig. 2, comparable cleavage patterns for apo- and holo-Trun-3 were obtained, indicating both similar digestion site accessibility and conformation, in agreement with results obtained by CD spectroscopy and DSC. However, a differential time-course of digestion was observed, as part of the holo-protein remained intact even after a one-hour treatment, while the apo-protein suffered a relatively faster proteolysis (Fig. 2A and B). The absence of the cofactor seems to introduce some plasticity on the tertiary structure, although does not negatively impact the overall protein fold. This flexibility is a likely prerequisite to enable the flavin to enter the interior of the apoprotein. Our data is consistent with studies on other flavoenzymes in which a more flexible structure is observed for deflavo enzymes giving rise, for example, to increase susceptibility to proteolysis in time [39].

Taken together, the present results indicate that apo-protein has a defined conformation, since the addition of FAD is not necessary to induce the conformational state of Trun-3. Apparently, the folded apo-enzyme is flexible enough to allow the entrance of the cofactor to the pre-organized binding pocket resulting in the active holo-enzyme. This mechanism for FAD binding was described in other flavoproteins [40]. In the case of dihydrolipoamide dehydrogenase E3 subunit from *E. coli*, the presence of FAD promotes subtle conformational rearrangements, although its initial presence appears not to be required to promote the correct folding [41]. There are other cases where the protein is able to autonomously adopt a folded native conformation, and as soon as enough cofactor becomes available, the apo-protein binds the flavin and forms the functional complex, as was observed with the long-chain *Anabaena* PCC7119 [42] and *Azotobacter vinelandii* [43] apo-flavodoxins. When the wild-type *Anabaena* protein is overexpressed and the cells are quickly harvested (in FMN limiting conditions), or when FMN binding defective apo-flavodoxin variants are expressed, large amounts of well-folded apo-protein were recovered [44].

3.2. Characterization of FAD binding to the apo-protein Trun-3

Information about flavin–protein interaction was scarce among NDH-2s. The binding of FAD to apo-Trun-3 was analyzed by fluorescence spectroscopy, either by keeping constant the flavin concentration and changing protein concentration or conversely.

Fig. 3A shows the changes elicited in the fluorescence emission spectrum of 10 μM FAD with increasing concentration of apo-Trun-3. The progressive increment of the fluorescence intensity is also accompanied by a blue-shifting of the emission maximum λ_{em}^{max}. In turn, Fig. 3B shows

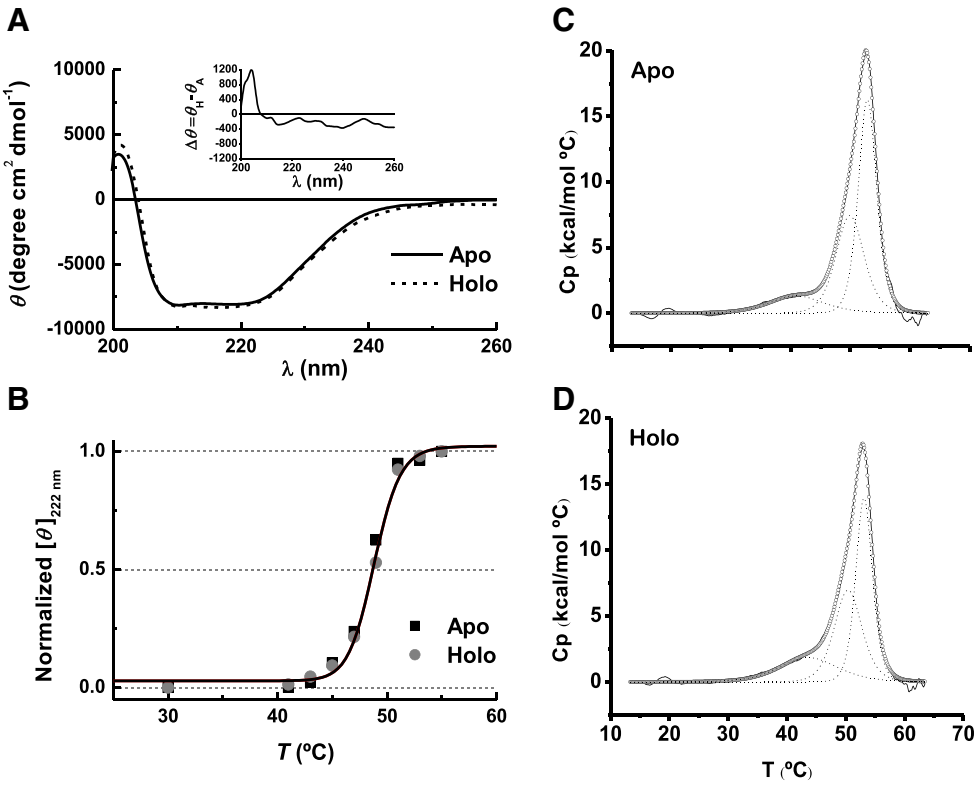

Fig. 1. FAD binding does not change apo-Trun-3 structure. (A) Far-UV CD spectra at 30 °C of apo-Trun-3 (solid line) and holo-Trun-3 (dotted line) in 50 mM potassium phosphate buffer, pH 7.5, containing 0.5 M NaCl. Data are expressed as mean molar residue ellipticity [θ], Eq. (1). Each CD spectrum was the average of five scans. Inset: differential CD spectrum between the holo- and apo-protein. (B) Thermal transition curves following ellipticity at 222 nm for apo- (■) and holo-Trun-3 (○). Values were normalized to the total change observed between 20 and 60 °C. Experiments were repeated three times and the average values are reported. The solid line represents the data fitting with the Boltzmann equation: $\theta = \theta_{min} + \frac{(\theta_{max}-\theta_{min})}{1+e^{(T_m-T)/\beta}}$. Differential scanning calorimetry thermograms of apo- (C) and holo-Trun-3 (D). DSC experimental data points (circles), best fit curves (solid line) and transitions obtained from the non-two-state transition model analyses (dotted lines) are shown. Crude thermograms were normalized by total protein concentration. Experiments were repeated three times and the average results are shown.

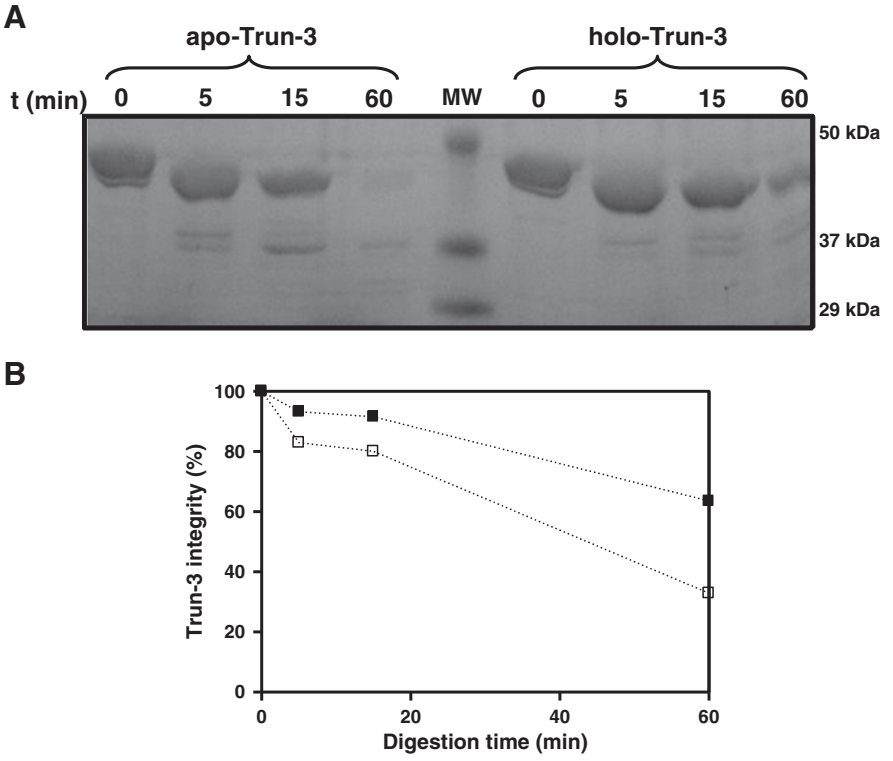

Fig. 2. FAD does not strongly impact the overall protein folding. Limited proteolysis with chymotrypsin experiments: (A) 10% SDS-PAGE of the apo- and holo-Trun-3 samples before digestion and digested fragments after 5 min, 15 min or 60 min. BIO-RAD low range pre-stained SDS-PAGE standards, MW 50, 37, and 29 kDa. Gel was stained with Coomassie Blue. (B) Quantification by gel densitometric analysis of apo- (□) and holo-Trun-3 (■) degradation during incubation with chymotrypsin. Representative results from three sets of experiments are shown.

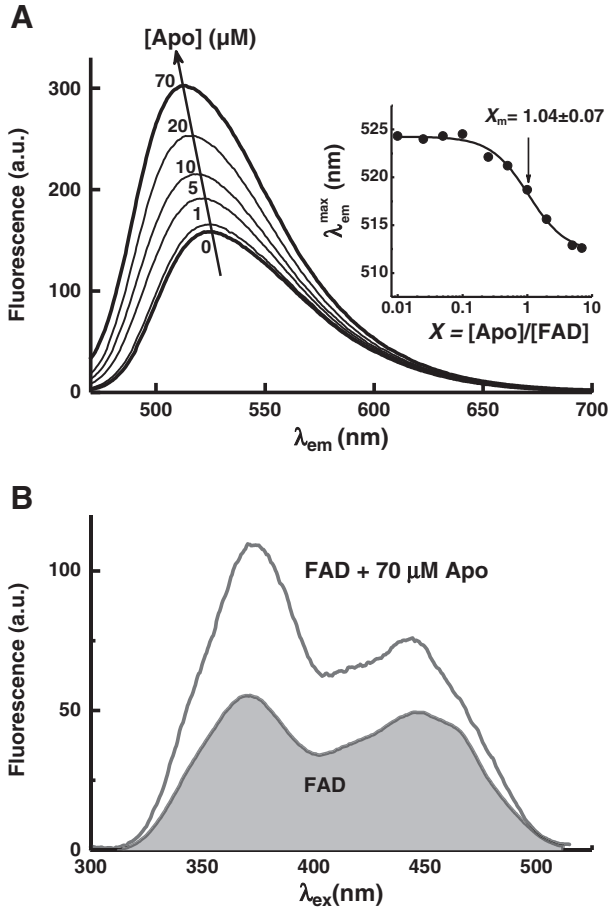

Fig. 3. FAD binding to apo-Trun-3 changes the surrounding environment of the flavin. Changes on the emission (A) and excitation (B) fluorescence spectra of FAD, elicited by the apo-protein Trun-3 in 50 mM potassium phosphate buffer, pH 7.5, containing 0.5 M NaCl. Inset of (A) represents the shifting of the emission maximum wavelength of FAD, λ_{em}^{max}, with the protein/flavin molar ratio $X = [Apo]/[FAD]$. The solid line is the data fitting with the Boltzmann equation: $\lambda = \lambda_{min} + \frac{(\lambda_{max}-\lambda_{min})}{1+e^{(X_m-X)/p}}$.

the variation of the fluorescence excitation spectrum of FAD, monitored with the emission wavelength fixed at 520 nm, by the addition of 70 μM of the apo-protein. Besides the almost twice fluorescence increment of the flavin upon binding, a modification in the intensity band ratio corresponding to the transitions from the ground state (S_0) to the lowest-lying excited states of the singlet manifold S_1 ($\lambda_{ab}^{max} \approx$ 442–450 nm) and S2 ($\lambda_{ab}^{max} \approx$ 360–375 nm) of the isoalloxazine chromophore was produced. All these spectral changes suggest a modification of the surrounding microenvironment sensed by FAD due to the interaction with the protein. This type of behavior for flavin derivatives is produced by the lack or displacement of hydrogen bonds formed between the isoalloxazine ring with solvent water molecules, as observed in the core of reversed micelles at very low water/surfactant molar ratios, where water molecules are highly immobilized [35], or in protein cavities, such as the blue-light receptor YtvA of *Bacillus subtilis*, in which the cofactor FMN is highly stabilized and immobilized by a hydrogen bond network involving several amino acids of the active site [45].

The inset of Fig. 3A shows the sigmoid-like behavior of the λ_{em}^{max} shifting with the protein/cofactor concentration ratio $X = [Apo]/[FAD]$, which midpoint value at $X_m \approx 1$ suggests a 1:1 binding stoichiometry upon formation of the holo-protein, according with the following association equilibrium, Eq. (6).

$$FAD + Apo \rightleftarrows Holo \quad K_A = \frac{[Holo]}{[FAD][Apo]} \tag{6}$$

The binding of FAD to apo-Trun-3 produced a parallel increment of both the fluorescence quantum yield (Φ_F^{FAD}) and the steady-state emission anisotropy (r^{FAD}) of FAD (Fig. 4A). It is worth to mention that the saturation value of $r^{FAD} = 0.207$, obtained by addition of high concentration of Trun-3, is close to that obtained for apo-protein alone ($r^{Apo} = 0.208$), calculated by measuring its intrinsic fluorescence emission at $\lambda_{em}^{max} = 335 \pm 5$ nm (data not shown). Assuming similar lifetimes for both the excited state of bound FAD and for the apo-Trun-3, this result suggests that the cofactor is tightly located into the protein, and the fluorescence depolarization of the flavin is mainly governed by the slower rotational diffusion of the whole protein backbone [46].

The increment of both Φ_F^{FAD} and r^{FAD} was recently reported for FAD dissolved in the core of sodium docusate (AOT) reverse micelles at low water content, e.g. $w_0 = [H_2O] / [AOT] \leq 6$, where the local viscosity is high enough to consider the flavin derivative almost immobilized inside the core of the reverse micelle [35]. A similar increase of fluorescence anisotropy of FAD was observed for the apo-protein PheA2, a flavin reductase component of phenol hydroxylase from *Bacillus thermoglucosidasius* A7 [47], indicating a strong interaction. Moreover, the Φ_F^{FAD} increment could be also the result of the preferential location of FAD in the binding site with an "open" conformation, as predicted by the reported PDB ID: 1OZK structure of the native *E. coli* NDH-2 [26] (Fig. 5), in which the intramolecular electron-transfer quenching of the excited state of the isoalloxazine ring by the adenine moiety is avoided [48].

The elicited changes of both fluorescence intensity and anisotropy can be used to estimate the association constant K_A of the equilibrium of Eq. (6). In the simplest scenario, only a single binding site or identical

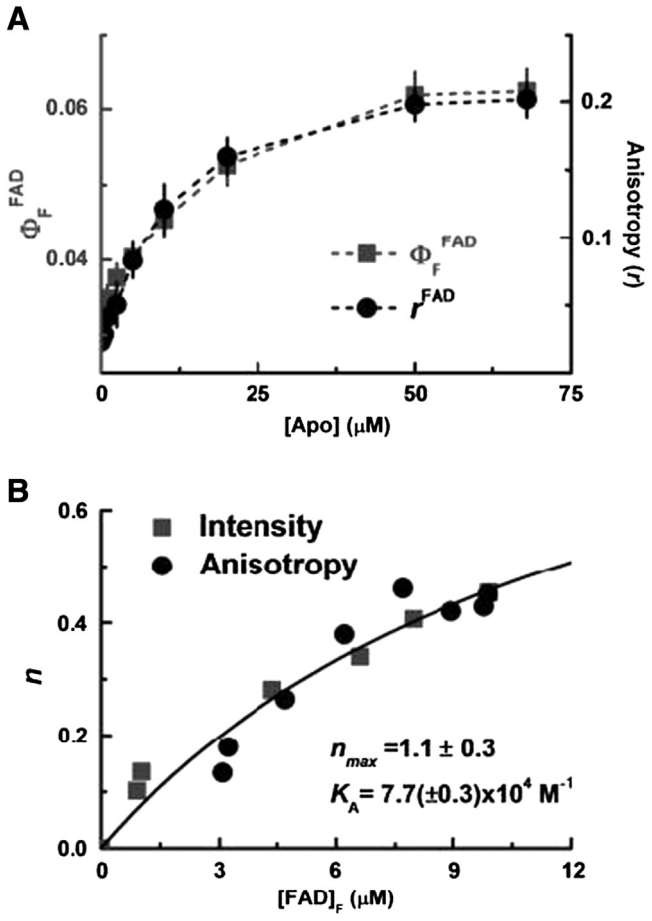

Fig. 4. FAD efficiently binds to apo-Trun-3. (A) Variation of the fluorescence quantum yield (Φ_F^{FAD}) and steady-state anisotropy (r^{FAD}) of FAD with the concentration of the apo-protein Trun-3. (B) Calculation of the association constant K_A and n of FAD to apo-Trun-3, Eq. (9), using steady-state fluorescence intensity (□) and anisotropy (●) values of FAD.

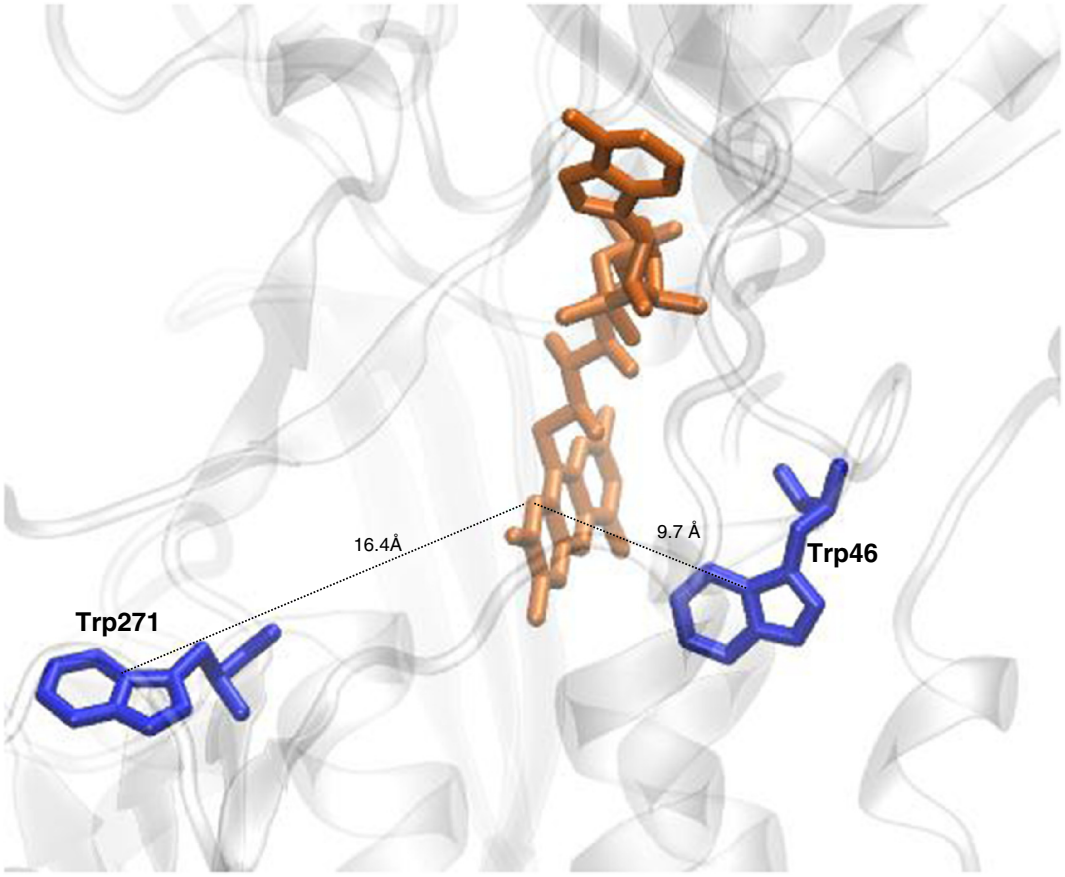

Fig. 5. FAD binds close to Trp residues of Trun-3. Ribbon representation of a portion of the NDH-2 three-dimensional model: FAD and tryptophan residues are colored in orange and blue, respectively. The diagram was created using the PDB file of NDH-2 theoretical model [24], with the program Visual Molecular Dynamics (VMD).

ideal sites in the protein will be considered. In this case, the overall fluorescence intensity (F) must be considered as the sum of the fluorescence intensity of the population of FAD molecules free in the aqueous pool $[FAD]_F$ and of that coming from the cofactor molecules bound to the protein $[FAD]_B$ [49]. Thus, the fraction of bound FAD (f_B) is defined as the ratio between $[FAD]_B$ (i.e. equivalent to the holo-protein concentration) and the total flavin concentrations $[FAD]_T$, Eq. (7), where F and F_0 are the measured fluorescence intensity of FAD in the presence and absence of apo-protein, and F_∞ is the fluorescence intensity of totally bounded FAD.

$$f_B = \frac{[FAD]_B}{[FAD]_F + [FAD]_B} = \frac{[Holo]}{[FAD]_T} = \frac{F - F_0}{F_\infty - F_0} \tag{7}$$

Because the fluorescence intensity of FAD increases upon binding, the calculation of f_B using the steady state anisotropy r is given by Eq. (8), where r_F and r_B are the anisotropies of the free and bound FAD, respectively, and $R = F_\infty / F_0$ is the fluorescence intensity correction factor under the same monochromator settings as the anisotropy measurement [46,50].

$$f_B = \frac{r - r_F}{R(r_B - r) + (r - r_F)} \tag{8}$$

Eqs. (7) and (8) assume the existence of only two states for the solute, e.g. bound and free, interacting with a single binding site N, irrespective of the protein concentration [49]. Therefore, the calculation of this parameter from both fluorescence intensity and anisotropy data allows the estimation of the average number of FAD molecules bound per protein molecule, $n = [FAD]_B / [Trun\text{-}3]_T$. As $[Trun\text{-}3]_T = [Apo] + [Holo]$, combining with K_A (Eq. (6)) and $[FAD]_F = (1 - f_B)[FAD]_T$, the hyperbolic function (Eq. (9)) for n is obtained.

$$n = \frac{n_{max} \cdot [FAD]_F}{K_A^{-1} + [FAD]_F} \tag{9}$$

In this case, the factor n_{max} was introduced as fitting variable to account the maximum value of cofactor molecules bound per protein molecule. According with the two pseudophase model proposed, a value of $n_{max} = 1$ must be expected [50]. Fig. 4B shows the variation of the specific binding ratio ν with $[FAD]_F$, and the non-linear fitting with Eq. (9) yields $K_A = 7.7 \times 10^4\ M^{-1}$ and $n_{max} \approx 1$, confirming the binding model proposed with a 1:1 stoichiometry upon formation of the holoprotein, as previously obtained from the sigmoidal fitting of the emission maximum shifting (inset of Fig. 3A).

Excitation at 295 nm of apo-Trun-3 shows the typical tryptophan-like emission with a maximum at 335 nm (Fig. 6A). This result indicates that the Trp residues are sensing a less polar environment than in aqueous solution [36], in agreement with the solvent-accessible surface area (SASA) analysis of the native *E. coli* NDH-2 computational model (PDB ID: 1OZK), which predicts that both tryptophan residues (Trp46 and Trp271) are buried in the protein [26,29]. The addition of FAD strongly quenched the protein fluorescence intensity, and after inner filter corrections with Eq. (2), it can be observed that no major spectral shift of the emission maximum was observed (Fig. 6A). Furthermore, the Stern–Volmer (SV) plot of $(F_0/F)_{corr}$ vs $[FAD]_T$ was perfectly linear (Fig. 6B). These results indicate that both Trp residues are accessible to the quencher as, in the case of a non-accessible Trp residue, the SV plot should show a downward curvature (saturation-like curve). Thus, the intrinsic fluorescence quenching of Trun-3 by FAD suggests that

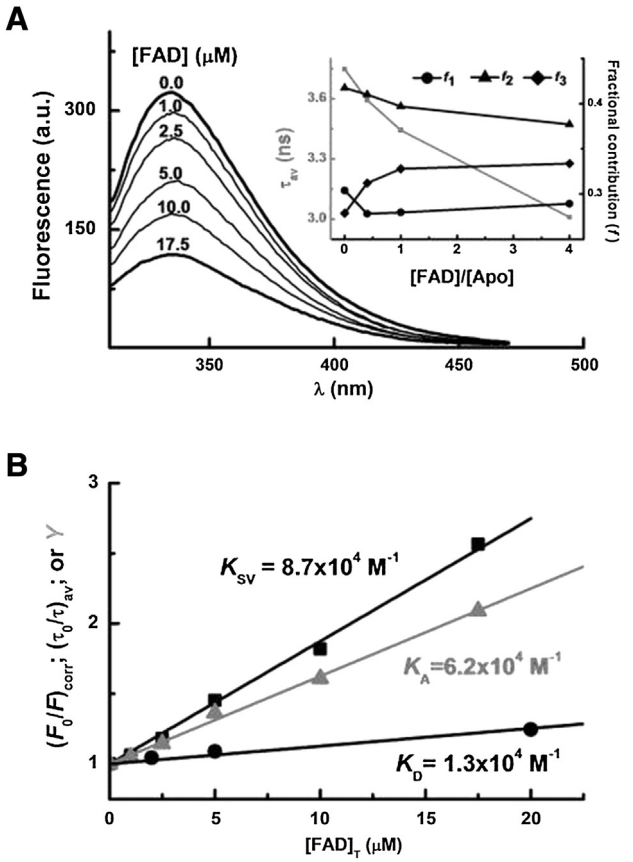

Fig. 6. FAD quenches almost statically the fluorescence of apo-Trun-3. (A) Fluorescence emission spectra of Trun-3 corrected by inner filter effects upon addition of FAD with Eq. (2). Inset: variation of the average fluorescence lifetime τ_{av} and fractional contribution f_i with the molar ratio [FAD]/[Apo]. (B) Stern–Volmer (SV) plots for the corrected fluorescence intensity $(F_0/F)_{corr}$ (■) and average lifetime $(\tau_0/\tau)_{av}$ (●) ratios, respectively, and for the corrected static quenching contribution $Y = [(F_0/F)_{corr}] / [(\tau_0/\tau)_{av}]$ (◀), Eq. (10).

the flavin cofactor can interact with both Trp residues in the binding site of the protein. In fact, estimation of the distance between the isoalloxazine ring of FAD to Trp46 and Trp271 from the 3D model of NDH-2 shows a closer location of FAD to both Trp residues (<17 Å) (Fig. 5). Thus, assuming similar protein conformation in solution, the proximity of FAD to both Trp residues of Trun-3 can be extrapolated.

In order to confirm this assumption, the fluorescence decay behavior of apo-Trun-3 was analyzed as a function of increasing FAD concentration by TCSPC (Time-Correlated Single Photon Counting) experiments with excitation at 280 nm and emission monitored at 340 nm. In the absence of FAD, the best deconvolution fitting of the decay was obtained using a three-exponential decay function (Eq. (4)), yielding individual lifetimes τ_i of 0.85, 3.32, and 7.53 ns with fluorescence fractional contributions f_i of 0.30, 0.42, and 0.28, respectively. From this lifetime distribution, an average lifetime of $\tau_{av} = 3.75$ ns was calculated with Eq. (5). Multi-exponential decay is a common feature either in single or multi-tryptophan containing proteins, mainly due to the conformational complexity and/or specific interaction of some amino acid residues that can act as quenchers [51]. Upon addition of FAD, the protein fluorescence decay was also well-fitted with the three-exponential decay function (data not shown). However, as all individual lifetimes were reduced with the flavin concentration, the fractional contributions f_1 and f_2 corresponding to the shorter and middle lifetimes were reduced up to a molar ratio [FAD]/[Apo] ≈ 1, while a parallel increase was observed for the f_3 value associated with the longest lifetime of the protein (inset of Fig. 6A). This saturation behavior of the fluorescence fractional contributions reached at [FAD]/[Apo] ≥ 1 can be associated with the 1:1 stoichiometry for the binding as described above. Thus, the combined variation of both τ_i and f_i resulted in a slight and progressive reduction of the average lifetime τ_{av} value. Once more, the dynamic quenching of all Trp fluorescence-like decay components of Trun-3 by FAD addition supports our previous assumption of closer location of the cofactor to the two Trp residues of the truncated protein.

Finally, both steady-state and dynamic fluorescence quenching of Trun-3 by FAD were analyzed, according to the classical SV relationship (F_0/F) or $(\tau_0/\tau) = 1 + K_{SV}[FAD]_T$, respectively, with K_{SV} (M^{-1}) as the SV quenching constant. For both $(F_0/F)_{corr}$ and $(\tau_0/\tau)_{av}$ ratios, satisfactory linear correlations with the total FAD concentration were fulfilled (Fig. 6B), and by comparing the slope difference between both SV-plots, it can be concluded that the quenching mechanism of Trun-3 by FAD is mainly static (see [36]). In fact, from the apparent dynamic component $K_{SV} = K_D = k_q\tau_{0,av} = 1.3 \times 10^4\ M^{-1}$, the bimolecular quenching constant $k_q = 3.5 \times 10^{12}\ M^{-1}\ s^{-1}$ was estimated. This k_q value exceeds, by almost three-order of magnitude, the rate constant value for bimolecular diffusion-controlled processes in water at room temperature ($\approx 6 \times 10^9\ M^{-1}\ s^{-1}$), suggesting that the dynamic quenching contribution $(\tau_0/\tau)_{av}$ is produced by transient and/or energy-transfer effects due to the close vicinity of FAD to the Trp residues into the binding site of apo-Trun-3 [51].

Usually, in the analysis of a solute binding efficiency by intrinsic fluorescence quenching of a protein, most articles consider a 100% static quenching mechanism, since the dynamic quenching component is ignored. This is based on the fact that its occurrence would require a quenching rate constant higher than that expected for diffusion controlled processes in homogeneous fluid solutions (i.e. $\approx 10^{10}\ M^{-1}\ s^{-1}$) (see review [52]). However, the SV-plot of Fig. 6B, obtained from fluorescence lifetime's analysis, clearly illustrates the occurrence of a minor contribution of dynamic quenching that affects the total fluorescence intensity ratio $(F_0/F)_{cor}$. Therefore, the $(F_0/F)_{corr}$ ratio obtained from intensity fluorescence measurements can be considered as the product between "pure" static and "apparent" dynamic quenching contributions, Eq. (10), where the association constant K_A (as defined in Eq. (6)) is only included in the static quenching contribution:

$$\left(\frac{F_0}{F}\right)_{corr} = (1 + K_A[FAD]_T) \times (1 + K_D[FAD]_T) = (1 + K_A[FAD]_T) \times \left(\frac{\tau_0}{\tau}\right)_{av}. \quad (10)$$

Thus, the dynamic quenching component can be easily corrected from $(F_0/F)_{corr}$ by plotting $Y = (F_0/F)_{corr} / (\tau_0/\tau)_{av}$ vs. $[FAD]_T$. A linear plot was obtained, according with a 1:1 stoichiometry of the complex formation, and a slope $K_A = 6.2\ (\pm 0.2) \times 10^4\ M^{-1}$. This K_A value is very close to that of $7.7 \times 10^4\ M^{-1}$ obtained by the fluorescence intensity and anisotropy enhancement of FAD as a function of Trun-3 concentration (Fig. 4), confirming the validity of the two approaches used.

4. Conclusions

For the first time, FAD binding properties to type II NADH dehydrogenase were characterized. Our strategy involved the use of the soluble truncated mutant Trun-3, which represents an excellent model for studying the protein/cofactor interactions, since eventual difficulties related to the use of the native membrane enzyme were avoided. As we described before, Trun-3 was obtained as a cytosolic apo-protein and the overall structural conformation of holo-Trun-3 resembles the *E. coli* NDH-2 wild-type protein [29]. The binding of the FAD cofactor to apo-Trun-3 did not induce significant changes in secondary and tertiary structures, suggesting that FAD was not required to promote the correct folding of NDH-2. The fact that Trun-3 structure was kept almost intact in the absence of the cofactor is in agreement with the fast reactivation process after FAD binding [28]. The FAD cofactor binding to apo-Trun-3 was determined, obtaining an average association constant value of $K_A = 7.0(\pm 0.8) \times 10^4\ M^{-1}$, which corresponds to a Gibbs free

energy $\Delta G^{\circ} \approx -28$ kJ/mol, a driven force consistent with a highly favorable protein–cofactor interaction. The incorporation of FAD into the soluble protein occurs with a 1:1 stoichiometry, in agreement with the results previously reported for native *E. coli* NDH-2 by Jaworowski et al. [23].

Acknowledgements

We specially thank Dr G.D. Fidelio and Dr M.I. Burgos for receiving J.M.V. at their laboratory and for helpful contribution in far UV-CD and DSC measurements. This research was supported by Argentinean grants of the Consejo Nacional de Investigaciones Científicas y Técnicas (CONICET-PIP's 6399/09 and 0374/12), Agencia de Promoción Científica y Tecnológica (ANPCyT-PICT 2012-2666), Universidad Nacional de Tucumán (UNT-CIUNT 26/D443), and Universidad Nacional de Santiago del Estero (UNSE-CICyT 23A/162). J.M.V. thanks CONICET for doctoral fellowship. F.E.M.V., C.D.B. and V.A.R. are research members of CONICET.

References

[1] E. Steensma, C.P. van Mierlo, Structural characterisation of apo-flavodoxin shows that the location of the stable nucleus differs among proteins with a flavodoxin-like topology, J. Mol. Biol. 282 (1998) 653–666.
[2] W.R. Fisher, H. Taniuchi, C.B. Anfinsen, On the role of heme in the formation of the structure of cytochrome c, J. Biol. Chem. 248 (1973) 3188–3195.
[3] E. Steensma, M.J. Nijman, Y.J. Bollen, P.A. de Jager, W.A. van den Berg, W.M. van Dongen, C.P. van Mierlo, Apparent local stability of the secondary structure of *Azotobacter vinelandii* holoflavodoxin II as probed by hydrogen exchange: implications for redox potential regulation and flavodoxin folding, Protein Sci. 7 (1998) 306–317.
[4] V. Joosten, W.J.H. van Berkel, Flavoenzymes, Curr. Opin. Chem. Biol. 11 (2007) 195–202.
[5] M.W. Fraaije, A. Mattevi, Flavoenzymes: diverse catalysts with recurrent features, Trends Biochem. Sci. 25 (2000) 126–132.
[6] S. Bornemann, Flavoenzymes that catalyse reactions with no net redox change, Nat. Prod. Rep. 19 (2002) 761–772.
[7] C.L. Ávila, V.A. Rapisarda, R.N. Farías, J. De Las Rivas, R. Chehín, Linear array of conserved sequence motifs to discriminate protein subfamilies: study on pyridine nucleotide-disulfide reductases, BMC Bioinforma. 8 (2007) 96.
[8] A.M. Melo, T.M. Bandeiras, M. Teixeira, New insights into type II NAD(P)H:quinone oxidoreductases, Microbiol. Mol. Biol. Rev. 68 (2004) 603–616.
[9] J. Fang, D.S. Beattie, Novel FMN-containing rotenone-insensitive NADH dehydrogenase from *Trypanosoma brucei* mitochondria: isolation and characterization, Biochemistry 41 (2002) 3065–3072.
[10] A.M. Michalecka, A.S. Svensson, F.I. Johansson, S.C. Agius, U. Johanson, A. Brennicke, S. Binder, A.G. Rasmusson, *Arabidopsis* genes encoding mitochondrial type II NAD(P)H dehydrogenases have different evolutionary origin and show distinct responses to light, Plant Physiol. 133 (2003) 642–652.
[11] P.R. Rich, A. Marechal, The mitochondrial respiratory chain, Essays Biochem. 47 (2010) 1–23.
[12] M.G. Matus-Ortega, K.G. Salmerón-Santiago, O. Flores-Herrera, G. Guerra-Sánchez, F. Martínez, J.L. Rendón, J.P. Pardo, The alternative NADH dehydrogenase is present in mitochondria of some animal taxa, Comp. Biochem. Physiol. Part D Genomics Proteomics 6 (2011) 256–263.
[13] N. Fisher, P.G. Bray, S.A. Ward, G.A. Biagini, The malaria parasite type II NADH:quinone oxidoreductase: an alternative enzyme for an alternative lifestyle, Trends Parasitol. 23 (2007) 305–310.
[14] C.K. Dong, V. Patel, J.C. Yang, J.D. Dvorin, M.T. Duraisingh, J. Clardy, D.F. Wirth, Type II NADH dehydrogenase of the respiratory chain of *Plasmodium falciparum* and its inhibitors, Bioorg. Med. Chem. Lett. 19 (2009) 972–975.
[15] G.A. Biagini, N. Fisher, A.E. Shone, M.A. Mubaraki, A. Srivastava, A. Hill, T. Antoine, A.J. Warman, J. Davies, C. Pidathala, R.K. Amewu, S.C. Leung, R. Sharma, P. Gibbons, D.W. Hong, B. Pacorel, A.S. Lawrenson, S. Charoensutthivarakul, L. Taylor, O. Berger, A. Mbekeani, P.A. Stocks, G.L. Nixon, J. Chadwick, J. Hemingway, M.J. Delves, R.E. Sinden, A.M. Zeeman, C.H. Kocken, N.G. Berry, P.M. O'Neill, S.A. Ward, Generation of quinolone antimalarials targeting the *Plasmodium falciparum* mitochondrial respiratory chain for the treatment and prophylaxis of malaria, Proc. Natl. Acad. Sci. U. S. A. 109 (2012) 8298–8303.
[16] T. Yano, L.S. Li, E. Weinstein, J.S. Teh, H. Rubin, Steady-state kinetics and inhibitory action of antitubercular phenothiazines on *Mycobacterium tuberculosis* type-II NADH-menaquinone oxidoreductase (NDH-2), J. Biol. Chem. 281 (2006) 11456–11463.
[17] J.S. Teh, T. Yano, H. Rubin, Type II NADH: menaquinone oxidoreductase of *Mycobacterium tuberculosis*, Infect. Disord. Drug Targets 7 (2007) 169–181.
[18] B.B. Seo, J. Wang, T.R. Flotte, T. Yagi, A. Matsuno-Yagi, Use of the NADH-quinone oxidoreductase (NDI1) gene of *Saccharomyces cerevisiae* as a possible cure for complex I defects in human cells, J. Biol. Chem. 275 (2000) 37774–37778.
[19] M.F. Maas, C.H. Sellem, F. Krause, N.A. Dencher, A. Sainsard-Chanet, Molecular gene therapy: overexpression of the alternative NADH dehydrogenase NDI1 restores overall physiology in a fungal model of respiratory complex I deficiency, J. Mol. Biol. 399 (2010) 31–40.
[20] M. Marella, B.B. Seo, T.R. Flotte, A. Matsuno-Yagi, T. Yagi, No immune responses by the expression of the yeast Ndi1 protein in rats, PLoS One 6 (2011) 25910.
[21] M. Marella, B.B. Seo, T. Yagi, A. Matsuno-Yagi, Parkinson's disease and mitochondrial complex I: a perspective on the Ndi1 therapy, J. Bioenerg. Biomembr. 41 (2009) 493–497.
[22] I.G. Young, B.L. Rogers, H.D. Campbell, A. Jaworowski, D.C. Shaw, Nucleotide sequence coding for the respiratory NADH dehydrogenase of *Escherichia coli*: UUG initiation codon, Eur. J. Biochem. 116 (1981) 165–170.
[23] A. Jaworowski, G. Mayo, D.C. Shaw, H.D. Campbell, I.G. Young, Characterization of the respiratory NADH dehydrogenase of *Escherichia coli* and reconstitution of NADH oxidase in *ndh* mutant membrane vesicles, Biochemistry 20 (1981) 3621–3628.
[24] Y. Feng, W. Li, J. Li, J. Wang, J. Ge, D. Xu, Y. Liu, K. Wu, Q. Zeng, J.W. Wu, C. Tian, B. Zhou, M. Yang, Structural insight into the type-II mitochondrial NADH dehydrogenases, Nature 491 (2012) 478–482.
[25] M. Iwata, Y. Lee, T. Yamashita, T. Yagi, S. Iwata, A.D. Cameron, M.J. Maher, The structure of the yeast NADH dehydrogenase (Ndi1) reveals overlapping binding sites for water- and lipid-soluble substrates, Proc. Natl. Acad. Sci. U. S. A. 109 (2012) 15247–15252.
[26] R. Schmid, D.L. Gerloff, Functional properties of the alternative NADH: ubiquinone oxidoreductase from *E. coli* through comparative 3-D modeling, FEBS Lett. 578 (2004) 163–168.
[27] V.A. Rapisarda, R.N. Chehín, J. De Las Rivas, L. Rodríguez-Montelongo, R.N. Farías, E.M. Massa, Evidence for Cu(I)-thiolate ligation and prediction of a putative copper-binding site in the *Escherichia coli* NADH dehydrogenase-2, Arch. Biochem. Biophys. 405 (2002) 87–94.
[28] J.M. Villegas, S.I. Volentini, M.R. Rintoul, V.A. Rapisarda, Amphipathic C-terminal region of *Escherichia coli* NADH dehydrogenase-2 mediates membrane localization, Arch. Biochem. Biophys. 505 (2011) 155–159.
[29] J.M. Villegas, C.M. Torres-Bugeau, R. Chehín, M.I. Burgos, G.D. Fidelio, M.R. Rintoul, V.A. Rapisarda, Maintenance and thermal stabilization of NADH dehydrogenase-2 conformation upon elimination of its C-terminal region, Biochimie 95 (2013) 382–387.
[30] G. Eggink, H. Engel, G. Vriend, P. Terpstra, B. Witholt, Rubredoxin reductase of *Pseudomonas oleovorans*. Structural relationship to other flavoprotein oxidoreductases based on one NAD and two FAD fingerprints, J. Mol. Biol. 212 (1990) 135–142.
[31] V.A. Rapisarda, L.R. Montelongo, R.N. Farías, E.M. Massa, Characterization of an NADH-linked cupric reductase activity from the *Escherichia coli* respiratory chain, Arch. Biochem. Biophys. 370 (1999) 143–150.
[32] O.H. Lowry, N.J. Rosebrough, A.L. Farr, R.J. Randall, Protein measurement with the Folin phenol reagent, J. Biol. Chem. 193 (1951) 265–275.
[33] U.K. Laemmli, Cleavage of structural proteins during the assembly of the head of bacteriophage T4, Nature 227 (1970) 680–685.
[34] J.B. Bertoldo, G. Razzera, J. Vernal, F.C. Brod, A.C. Arisi, H. Terenzi, Structural stability of *Staphylococcus xylosus* lipase is modulated by $Zn(2^{+})$ ions, Biochim. Biophys. Acta 1814 (2011) 1120–1126.
[35] L. Valle, F.E.M. Vieyra, C.D. Borsarelli, Hydrogen-bonding modulation of excited-state properties of flavins in a model of aqueous confined environment, Photochem. Photobiol. Sci. 11 (2012) 1051–1061.
[36] J.R. Lakowicz, Principles of Fluorescence Spectroscopy, 3st edn Springer Science + Business Media, LLC, Singapore, 2006.
[37] S.M. Kelly, T.J. Jess, N.C. Price, How to study proteins by circular dichroism, Biochim. Biophys. Acta 1751 (2005) 119–139.
[38] U.B. Ericsson, B.M. Hallberg, G.T. DeTitta, N. Dekker, P. Nordlund, Thermofluor-based high-throughput stability optimization of proteins for structural studies, Anal. Biochem. 357 (2006) 289–298.
[39] G.T. Tarelli, M.A. Vanoni, A. Negri, B. Curti, Characterization of a fully active N-terminal 37-kDa polypeptide obtained by limited tryptic cleavage of pig kidney D-amino acid oxidase, J. Biol. Chem. 265 (1990) 21242–21246.
[40] M.W. Fraaije, R.H. van Den Heuvel, W.J. van Berkel, A. Mattevi, Structural analysis of flavinylation in vanillyl-alcohol oxidase, J. Biol. Chem. 275 (2000) 38654–38658.
[41] H. Lindsay, E. Beaumont, S.D. Richards, S.M. Kelly, S.J. Sanderson, N.C. Price, J.G. Lindsay, FAD insertion is essential for attaining the assembly competence of the dihydrolipoamide dehydrogenase (E3) monomer from *Escherichia coli*, J. Biol. Chem. 275 (2000) 36665–36670.
[42] J. Fernández-Recio, C.G. Genzor, J. Sancho, Apoflavodoxin folding mechanism: an alpha/beta protein with an essentially off-pathway intermediate, Biochemistry 40 (2001) 15234–15245.
[43] Y.J. Bollen, I.E. Sánchez, C.P. van Mierlo, Formation of on- and off-pathway intermediates in the folding kinetics of *Azotobacter vinelandii* apoflavodoxin, Biochemistry 43 (2004) 10475–10489.
[44] J. López-Llano, S. Maldonado, S. Jain, A. Lostao, R. Godoy-Ruiz, J.M. Sanchez-Ruiz, M. Cortijo, J. Fernández-Recio, J. Sancho, The long and short flavodoxins: II. The role of the differentiating loop in apoflavodoxin stability and folding mechanism, J. Biol. Chem. 279 (2004) 47184–47191.
[45] S. Raffelberg, M. Mansurova, W. Gärtner, A. Losi, Modulation of the photocycle of a LOV domain photoreceptor by hydrogen-bonding network, J. Am. Chem. Soc. 113 (2011) 5346–5356.
[46] C.M. Ingersoll, C.M. Strollo, Steady-state fluorescence anisotropy to investigate flavonoids binding to proteins, J. Chem. Educ. 84 (2007) 1313–1315.
[47] R.H. van den Heuvel, A.H. Westphal, A.J. Heck, M.A. Walsh, S. Rovida, W.J. van Berkel, A. Mattevi, Structural studies on flavin reductase PheA2 reveal binding of NAD in an unusual folded conformation and support novel mechanism of action, J. Biol. Chem. 279 (2004) 12860–12867.
[48] G.F. Li, K.D. Glusac, The role of adenine in fast excited-state deactivation of FAD: a femtosecond mid-IR transient absorption study, J. Phys. Chem. B 113 (2009) 9059–9061.

[49] E. Alarcón, A. Aspée, E.B. Abuin, E.A. Lissi, Evaluation of solute binding to proteins and intra-protein distances from steady state fluorescence measurements, J. Photochem. Photobiol. B Biol. 106 (2012) 1–17.
[50] D.A. Malencik, S.R. Anderson, Peptide binding by calmodulin and its proteolytic fragments and by troponin-C, Biochemistry 23 (1984) 2420–2428.
[51] Y. Engelborghs, The analysis of time resolved protein fluorescence in multi-tryptophan proteins, Spectrochim. Acta A Mol. Biomol. Spectrosc. 57 (2001) 2255–2270.
[52] M. van de Weert, L. Stella, Fluorescence quenching and ligand binding: a critical discussion of a popular methodology, J. Mol. Struct. 998 (2011) 144–150.